A two-compartment model of pulmonary nitric oxide exchange dynamics

NIKOLAOS M. TSOUKIAS AND STEVEN C. GEORGE
Department of Chemical and Biochemical Engineering and Materials Science,
University of California at Irvine, Irvine, California 92697-2575

Tsoukias, Nikolaos M., and Steven C. George. A two-compartment model of pulmonary nitric oxide exchange dynamics. *J. Appl. Physiol.* 85(2):653–666, 1998.—The relatively recent detection of nitric oxide (NO) in the exhaled breath has prompted a great deal of experimentation in an effort to understand the pulmonary exchange dynamics. There has been very little progress in theoretical studies to assist in the interpretation of the experimental results. We have developed a two-compartment model of the lungs in an effort to explain several fundamental experimental observations. The model consists of a nonexpansile compartment representing the conducting airways and an expansile compartment representing the alveolar region of the lungs. Each compartment is surrounded by a layer of tissue that is capable of producing and consuming NO. Beyond the tissue barrier in each compartment is a layer of blood representing the bronchial circulation or the pulmonary circulation, which are both considered an infinite sink for NO. All parameters were estimated from data in the literature, including the production rates of NO in the tissue layers, which were estimated from experimental plots of the elimination rate of NO at end exhalation (E_{NO}) vs. the exhalation flow rate ($\dot{V}_E$). The model is able to simulate the shape of the NO exhalation profile and to successfully simulate the following experimental features of endogenous NO exchange: *1*) an inverse relationship between exhaled NO concentration and $\dot{V}_E$, *2*) the dynamic relationship between the phase III slope and $\dot{V}_E$, and *3*) the positive relationship between E_{NO} and $\dot{V}_E$. The model predicts that these relationships can be explained by significant contributions of NO in the exhaled breath from the nonexpansile airways and the expansile alveoli. In addition, the model predicts that the relationship between E_{NO} and $\dot{V}_E$ can be used as an index of the relative contributions of the airways and the alveoli to exhaled NO.

mathematical model; elimination rate; phase III; single exhalation

THE IMPORTANCE OF NITRIC OXIDE (NO) in the physiology of lung function has steadily increased in the past decade. Experimental work has dominated this influx of information and has provided critical information related to the cellular source of NO in the lungs, the specific physiological functions, and the detection of endogenous NO in the exhaled breath. On the basis of the ability of NO to relax smooth muscle, there has been interest in using exogenous NO delivered by inhalation as a therapy in such diseases as pulmonary hypertension, acute respiratory distress syndrome, and bronchial asthma. In addition, there has been interest in using endogenously exhaled NO levels as a noninvasive index of pulmonary inflammation (13). This interest has generated a need to understand the exchange dynamics of NO within the lungs.

The exchange dynamics of NO in the lungs are different from those of other previously studied endogenous gases such as O_2 and CO_2 because of specific differences in physical and biochemical properties. *1*) NO, with 11 valence electrons, is a free radical and is reactive with a number of different endogenous substrates, including O_2, superoxide, thiols, and metalloproteins. The presence of this array of substrates results in a half-life ($t_{1/2}$) of free NO in vivo that is ~0.5–15 s, depending on the specific physiological state (5, 16). *2*) NO is actively produced basally and in response to various stimuli, such as cytokines, by the cells that comprise the alveolar and airway regions of the lungs. *3*) NO binds avidly to hemoglobin in the blood, the kinetics of which are much different from those of CO_2 and O_2, but may play an important role in the local control of oxygenation (12). Theoretical modeling has historically played an important role in our understanding of pulmonary gas exchange dynamics; however, because of the unique biochemical features of NO, new models must be developed to complete our understanding of NO exchange. The lone attempt to model NO exchange in the lungs lumped the entire lung into a single compartment that effectively represented the alveolar region (11). This model was a starting point for modeling NO exchange dynamics and provided some initial insight into NO exchange. However, much further work is needed, inasmuch as a single-compartment model is not capable of describing the growing experimental evidence that exhaled endogenous NO is derived from an alveolar and an airway source. The alveoli and airways are two distinct regions of the lungs with many different features. From a gas-exchange perspective, perhaps the most important is the fact that the alveolar volume is expansile and the airway volume is relatively nonexpansile. The goal of this study is to develop a relatively simple two-compartment model of NO exchange dynamics that can *1*) describe the basic features of NO exchange dynamics previously observed experimentally by us (26) and by others (20, 24), *2*) provide initial insight into the exchange properties of exogenous NO, and *3*) provide direction for future experimentation.

MODEL DEVELOPMENT

General Structure

A model of the human lungs was developed (Fig. 1) that includes enough detail to describe the following basic features of NO exchange observed experimentally: *1*) breath holding before exhalation creates an initial spike in NO concentration during exhalation of the airway volume, *2*) exhaled NO concentration is an inverse function of exhalation flow rate ($\dot{V}_E$), and *3*) elimination rate of NO from the lungs (E_{NO}) is a positive function of $\dot{V}_E$. These basic observations are consistent
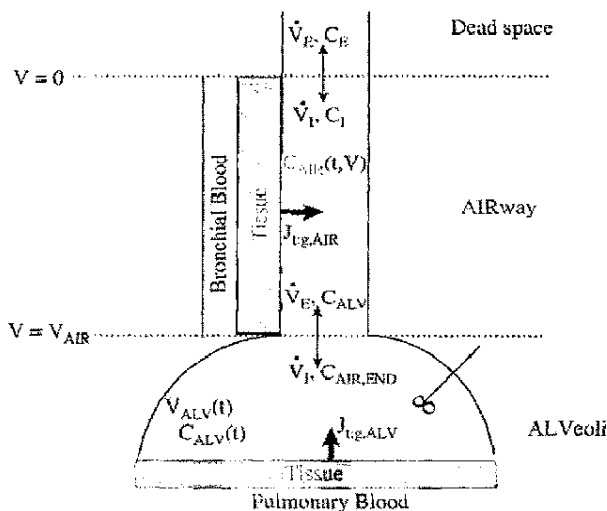
Fig. 1. Schematic of 2-compartment model for nitric oxide (NO) pulmonary exchange. First compartment represents relatively nonexpansile conducting airways; second compartment represents expansile alveoli. Each compartment is adjacent to a layer of tissue that is capable of producing and consuming NO. Exterior to tissue is a layer of blood that represents bronchial or pulmonary circulation and serves as an infinite sink for NO. $\dot{V}_E$ and $\dot{V}_I$, expiratory and inspiratory flow, respectively; C_E and C_I, expiratory and inspiratory concentration, respectively; C_{air} and C_{alv}, airway and alveolar concentration, respectively; V_{air} and V_{alv}, airway and alveolar volume, respectively; $J_{t:g,air}$ and $J_{t:g,alv}$, total flux of NO from tissue to air and from alveolar tissue, respectively; t, time; V, volume.

with the alveolar and the airway regions of the lungs as sources of exhaled NO. Hence, the model (Fig. 1) consists of two main compartments: 1) a rigid or nonexpansile compartment representing the conducting zone or airways [trachea through *generation 17* as defined by Weibel (27)] and 2) a flexible or expansile compartment representing the respiratory bronchioles and alveolar region (*generation 18* and beyond). Both compartments are surrounded by a layer of tissue representing the bronchial mucosa in the airway compartment and the alveolar membrane in the alveolar compartment. Blood representing the bronchial circulation and the pulmonary circulation is distal to the tissue in the airway compartment and alveolar compartment, respectively. Cells present in the airway mucosa and the alveolar membrane are capable of producing endogenous NO (8, 23); hence, we assume that NO is produced at a constant rate per unit volume of tissue by the tissue surrounding the airway and alveolar compartments. The endogenously produced NO can follow one of three paths: 1) consumption through reaction with substrates within the tissue compartments, 2) diffusion toward the pulmonary or bronchial circulations, where it reacts instantaneously and irreversibly with the hemoglobin of the blood, or 3) diffusion toward the airstream, where it evaporates and enters the alveolar volume or airway volume. Consequently, there will be a net flux of NO between the tissue and the airstream in both compartments. The direction of the flux depends on the relative concentrations of NO in the tissue and

gas phases. Hence, NO concentration in the exhaled breath will depend on two additive mechanisms: 1) the exchange of NO in the alveolar compartment and 2) the conditioning of the alveolar gas as it is convected through the airway compartment. On the basis of this general structure, a series of mass balances on the tissue and gas phase of the airway compartment and the alveolar compartment produce the governing equations for the model.

Airway Compartment

Tissue phase. The airway compartment is modeled as a cylindrical tube, and the surrounding tissue (Fig. 2) is modeled as a homogenous compartment of uniform thickness ($L_{t,air}$) with aqueous physical properties. NO is produced uniformly in position and constant in time by the tissue at a rate $S_{t,air}$ (mol·s^{-1}·cm^{-3}). NO reacts with several substrates including O_2, superoxide, thiols, and metalloproteins such as guanylate cyclase (5); hence, NO is consumed by chemical reaction at a rate $R_{t,air}$ (mol·s^{-1}·cm^{-3}). The reaction with O_2 is second order in NO concentration, and this reaction is the rate-limiting step in the reaction with endogenous thiols such as glutathione (14). At physiological NO concentrations, only the reactions with superoxide and metalloproteins are significant (2); both are first order in NO concentration. Hence, the $R_{t,air}$ can be expressed as $kC_t(t, x, z)$, where k is an overall first-order rate constant (s^{-1}), $C_t(t, x, z)$ is the concentration of NO in the airway tissue, x is the distance from the bronchial blood compartment, z is the axial position, and t is time (s).
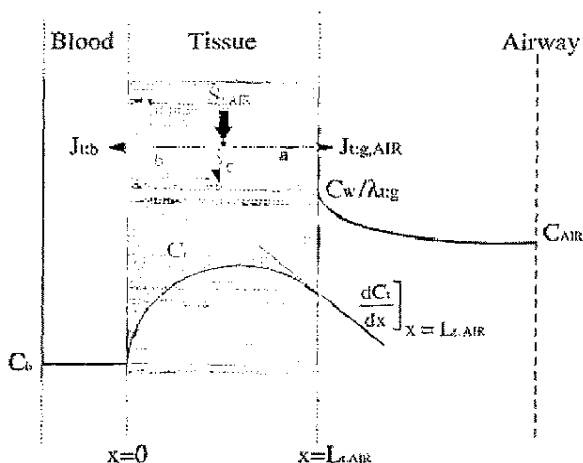

Fig. 2. Schematic of tissue layer in airway compartment. NO is produced from cellular sources at a constant rate in position and time ($S_{t,air}$). NO can then be transported by diffusion and enter bronchial circulation or gas phase of airway lumen, or it can be consumed by chemical reaction that is 1st order in NO concentration. Solid line, approximate radial concentration profile of NO in blood (b), tissue (t), and gas (g) phases under ambient inspired conditions. Radial gradient in NO concentration at tissue-air interface is proportional to flux of NO into airstream. $L_{t,air}$, thickness of tissue surrounding airway compartment; $\lambda_{t:g}$, partition coefficient of NO between tissue and air; C_w, concentration at airway-tissue interface; C_t, concentration in tissue.

The transport of NO from the site of production to the bronchial blood or the airstream occurs by molecular diffusion described by Fick's first law. The axial and angular gradients of NO concentration in the tissue are considered negligible. Hence, the transport of NO in the tissue can be sufficiently described by a one-dimensional diffusion equation. The small tissue thickness in comparison with the airway radius allows the use of simple Cartesian coordinates. Because of the fast reaction of the NO with hemoglobin present in abundance

Once the concentration profile in the tissue is known, using Fick's first law of diffusion, one can easily determine that the flux of NO from the tissue to the air ($J_{t:g,air}$) is a linear function of C_w

$$J_{t:g,air} = -D_t \frac{\partial C_t}{\partial x}\bigg|_{x=L_{t,air}} = a - b * C_w \qquad (4a)$$

where

$$a = \frac{D_t}{\beta}\left[\frac{1 - e^{-L_{t,air}/\beta}}{e^{L_{t,air}/\beta} - e^{-L_{t,air}/\beta}}\left(\frac{\dot{S}_{t,air}}{k}\right)(e^{L_{t,air}/\beta} + e^{-L_{t,air}/\beta}) - \frac{\dot{S}_{t,air}}{k}e^{-L_{t,air}/\beta}\right] \qquad (4b)$$

in the blood, the concentration of free NO at the interface between the blood and the tissue will be very close to zero. For the interface between the airway lumen and the tissue, we assume instant thermodynamic equilibrium governed by Henry's law. Under these assumptions, a differential mass balance of NO in the tissue produces the following second-order partial differential equation

$$D_t \frac{\partial^2 C_t}{\partial x^2} + \dot{S}_{t,air} - kC_t = \frac{\partial C_t}{\partial t} \qquad (1)$$

with the following boundary conditions: $C_t(t, 0) = 0$, $C_t(t, L_{t,air}) = C_w(t, z)$. D_t is the molecular diffusion coefficient of NO in tissue (3.3×10^{-5} cm²/s) (16), and C_w is the concentration of NO at the interface between the airway and tissue. $C_w(t, z)$ will depend on the concentration in the gas phase; as a result, $Eq.\ 1$ must be solved simultaneously with the NO mass balance in the gas phase of the airway compartment (see below). The solution to $Eq.\ 1$ can be simplified by assuming that C_t is in the steady state. This approximation is valid if the times of inspiration and expiration are much greater than ~0.6 s (the time for the concentration profile in the tissue to reach 90% of its steady-state value). This is due to the relatively small thickness of tissue relative to the rate of diffusion, and a proof is provided in APPENDIX A. With the assumption of steady state in the tissue, $Eq.\ 1$ reduces to

$$D_t \frac{\partial^2 C_t}{\partial x^2} + \dot{S}_{t,air} - kC_t = 0 \qquad (2)$$

The solution of $Eq.\ 2$ is

$$C_t(x) = \alpha(e^{x/\beta} - e^{-x/\beta}) + \frac{\dot{S}_{t,air}}{k}(1 - e^{-x/\beta}) \qquad (3a)$$

where

$$\alpha = \frac{1}{e^{L_{t,air}/\beta} - e^{-L_{t,air}/\beta}}C_w + \frac{-1 + e^{-L_{t,air}/\beta}}{e^{L_{t,air}/\beta} - e^{-L_{t,air}/\beta}}\left(\frac{\dot{S}_{t,air}}{k}\right) \qquad (3b)$$

$$\beta = \sqrt{\frac{D_t}{k}} \qquad (3c)$$

$$b = \frac{D_t}{\beta}\left[\frac{1}{e^{L_{t,air}/\beta} - e^{-L_{t,air}/\beta}}(e^{L_{t,air}/\beta} + e^{-L_{t,air}/\beta})\right] \qquad (4c)$$

Because of the very low solubility of NO in water and tissue, the radial transport of NO is not limited by diffusion in the gas phase (APPENDIX B) (6). Hence, $Eq.\ 4$ becomes

$$J_{t:g,air} = a - b * (\lambda_{t:g}C_{air}) \qquad (5)$$

where $\lambda_{t:g}$ is the partition coefficient of NO between the tissue and the air at 37°C and C_{air} is the bulk gas concentration of NO in the airway lumen. From $Eq.\ 5$, the flux of NO per unit airway surface area and per unit time between the airway tissue and the airway lumen is a linear function of the bulk gas concentration. As the concentration in the bulk gas of the airway lumen increases, the amount of NO that is consumed by the pulmonary blood or through reactions with substrates in the airway tissue increases; thus $J_{t:g,air}$ decreases. For C_{air} greater than $a/(b\lambda_{t:g})$, the consumption overcomes the endogenous production rates, resulting in net flux of NO from the airway to the tissue.

Gas phase. The airway compartment is modeled as a cylinder of constant total volume V_{air} and total surface area $A_{s,air}$. As described above, the absorption of NO by the airstream per unit surface area at any given point of the airway is described by $Eq.\ 5$. If we assume plug flow (i.e., no radial gradient in the velocity or concentration), then a differential mass balance of NO over a unit volume will give

$$-\dot{V}\frac{\partial C_{air}}{\partial z} + J_{t:g,air}A_s = A_c\frac{\partial C_{air}}{\partial t} \qquad (6a)$$

which can be transformed to a more convenient form by substituting $dV = dzA_c$

$$-\dot{V}\frac{\partial C_{air}}{\partial V} + J_{t:g,air}\left(\frac{A_s}{A_c}\right) = \frac{\partial C_{air}}{\partial t} \qquad (6b)$$

where $\dot{V}$ is volumetric flow rate of air ($\dot{V}_I$ for inspiration and $\dot{V}_E$ for expiration), A_s is the wall surface area per unit axial distance, A_c is airway volume per unit axial distance, and V is axial position in units of cumulative

volume. The ratio A_s/A_c (surface area per unit airway volume) increases in the human lung as the radius of each airway branch (r) decreases with generation number ($A_s/A_c = 2/r$). Hence, a more realistic description of the airway compartment is not as a perfect cylinder with constant A_s/A_c but, rather, as a cylinder whereby A_s/A_c increases with increasing axial position (or decreasing radius). To preserve an analytic solution to the model equations, A_s/A_c is approximated by a linear function of V ($R^2 = 0.94$) with use of the airway dimension data of Weibel (28): $A_s/A_c = a_I + b_IV$ for inspiration and $A_s/A_c = a_E + b_EV$ for expiration ($a_E = a_I + b_IV_{alr}$, $b_E = -b_I$). Hence, the total surface area of the airway compartment ($A_{s,air}$) is described by

$$A_{s,air} = \int_0^{V_{alr}} \left(\frac{A_s}{A_c}\right) dV \qquad (7)$$

Equation 6 is subject to the following arbitrary initial and boundary conditions: $C_{air}(0, V) = f(V)$ and $C_{air}(t, 0) = g(t)$, where $f(V)$ is the concentration profile of NO in the upper compartment before the inspiration (V = 0 at the mouth) or expiration (V = 0 at the entrance of the alveolar compartment) and $g(t)$ is the inspired concentration or the alveolar concentration for inspiration (I) or expiration (E), respectively. The solution to *Eq. 6* for constant V is

$$C_{air}(t, V) = \left[f(V - \dot{V}t) - \frac{a}{b\lambda_{t:g}}\right]e^{-b\lambda_{t:g}\gamma t} + \frac{a}{b\lambda_{t:g}} \qquad (8a)$$

for *case I* ($t < V/\dot{V}$) and

$$C_{air}(t, V) = \left[g(t - V/\dot{V}) - \frac{a}{b\lambda_{t:g}}\right]e^{-b\lambda_{t:g}\delta(V/\dot{V})} + \frac{a}{b\lambda_{t:g}} \qquad (8b)$$

for *case II* ($t > V/\dot{V}$), where

$$\gamma(t, V, j) = a_j + b_j(V - \dot{V}t/2) \qquad (8c)$$

$$\delta(V, j) = a_j + b_jV/2 \qquad j = 1, E \qquad (8d)$$

Case I describes the convective emptying of the airways at the beginning of inspiration or expiration; *case II* describes the convection of the alveolar gas or inspired gas through the airway compartment during expiration or inspiration, respectively. For the linearly increasing and decreasing flow rate maneuvers, V_E is not constant. However, an analytic solution is still attainable and is presented in APPENDIX C.

Alveolar Compartment

Gas phase. In modeling the alveolar region (Fig. 1), we assume a well-mixed compartment of variable volume [$V_{alv}(t)$]. The NO concentration in the alveolar gas [$C_{alv}(t)$] is uniform in position but is time dependent. NO can enter or leave the compartment through convective flow during inspiration or expiration, respectively, and can exchange with the alveolar tissue by diffusion. After an analysis that is identical to that presented for the airway tissue compartment, it can be shown that the flux of NO between the alveolar gas and the tissue

phase ($J_{t:g,alv}$) is a linear function of the bulk gas phase concentration (see *Eq. 5*). Then the net total flux (mol/s) of NO from the alveolar tissue ($J_{t:g,alv} A_{s,alv}$, where $A_{s,alv}$ is the surface area of the alveolar region) can be described by a combination of two terms

$$J_{t:g,alv} A_{s,alv} = \dot{S}_{app,alv} - DL_{NO}C_{alv} \qquad (9)$$

where $\dot{S}_{app,alv}$ (mol/s) is the apparent production rate of NO is the tissue (defined as the flux of NO into the alveolar compartment if the concentration of NO was zero in the compartment) and DL_{NO} is the diffusing capacity (mol·s⁻¹·mol⁻¹·cm³) of NO in the alveolar region. The method for determining the alveolar flux contrasts with that used in the airway compartment only in the manner of determining the coefficients of the linear function (i.e., $\dot{S}_{app,alv}$ and DL_{NO} in *Eq. 9*). In the alveolar compartment the coefficients can be determined experimentally rather than calculated from the geometric characteristics of the alveolar tissue and the endogenous production rate, as was done in the airway compartment. DL_{NO} has been experimentally measured (3, 7) and is equal to ~2,100 mol·s⁻¹·mol⁻¹·cm³, and $\dot{S}_{app,alv}$ can be determined from the steady-state alveolar concentration (see *Eq. 12*).

A differential mass balance for NO in the alveolar compartment (valid for inspiration and expiration) is then

$$V_{alv}(t) \frac{dC_{alv}}{dt} \qquad (10)$$

$$= (\dot{S}_{app,alv} - DL_{NO}C_{alv}) + \dot{V}_I(C_{air,end} - C_{alv})$$

subject to the following initial condition: $C_{alv}(0) = C_{alv,0}$. $V_{alv}(t)$ is the volume of the alveolar compartment, and $C_{air,end}$ is the concentration of NO in the air that exits the airway compartment. The volume change due to exchange of the respiratory gases has been neglected. *Equation 10* is valid for inspiration and expiration ($\dot{V}_I = 0$) as well as for nonconstant flow rates. The analytic solution of *Eq. 10* for constant flow rates and for constant $C_{air,end}$ is as follows

$$C_{alv}(t) = C_{alv}(0)\left[\frac{V_{alv}(0)}{V_{alv}(t)}\right]^{\xi+1}$$
$$+ \frac{\dot{S}_{app,alv} + \dot{V}_IC_{air,end}}{DL_{NO} + \dot{V}_I}\left\{1 - \left[\frac{V_{alv}(0)}{V_{alv}(t)}\right]^{\xi+1}\right\} \qquad (11a)$$

for *case I* (inspiration)

$$C_{alv}(t) = C_{alv}(0)\left[\frac{V_{alv}(t)}{V_{alv}(0)}\right]^{\xi} + \frac{\dot{S}_{app,NO}}{DL_{NO}}\left\{1 - \left[\frac{V_{alv}(t)}{V_{alv}(0)}\right]^{\xi}\right\} \qquad (11b)$$

for *case II* (expiration), where $\xi = DL_{NO}/\dot{V}_j$ (j = I or E), and

$$C_{alv}(t) = C_{alv}(0)e^{-[DL_{NO}/V_{alv}(t)]t}$$
$$+ \frac{\dot{S}_{app,alv}}{DL_{NO}}[1 - e^{-[DL_{NO}/V_{alv}(t)]t}] \qquad (11c)$$

for *case III* (breath hold). Solution of *Eq. 10* for linearly time-dependent expiratory flow rate is derived in APPENDIX D.

Parameter Estimation

Table **1** summarizes the values for key parameters used in the model simulations. The $\lambda_{t:g}$ is calculated from Henry's law constant for NO between air and water (25.8×10^6 mmHg NO · mol NO^{-1} · mol H$_2$O) (18a). The reaction constant k is calculated from the $t_{1/2}$ of NO in tissue. For first-order reactions, $k = \ln(2)/t_{1/2}$. The values of $t_{1/2}$ that have been reported in the literature range from 0.5 to 15 s, depending on the tissue and local environment (15, 16, 28). For our simulation, we chose an intermediate value of 4 s. The volume and the surface area of the upper compartment are calculated from Weibel's anatomic data (28) between the trachea and *generation 17*. The coefficients of the linear regression of the ratio A_s/A_c were chosen to satisfy *Eq. 7*. $\dot{S}_{app,alv}$ and $\dot{S}_{t,air}$ are more challenging to estimate. $\dot{S}_{app,alv}$ can be estimated from the diffusing capacity of NO and the expired steady-state alveolar concentration ($C_{alv,ss}$, *Eq. 10*) if $C_{alv,ss}$ is known

$$\dot{S}_{app,alv} = DL_{NO}C_{alv,ss} \qquad (12)$$

Hyde et al. (11) used the end-exhaled concentration of NO after a 15-s breath hold as an estimate of $C_{alv,ss}$. However, this approximation is valid only if the contribution from the airways is neglected [recall that the model of Hyde et al. (11) had only an expansile alveolar compartment]. An alternative technique, which accounts for the contribution from the airways, is to use E_{NO} from the lungs, as described in the companion article (27)

$$E_{NO} = \dot{V}_{E,ee}C_{alv,ee} + \bar{J}_{t:g,air}A_{s,air} \qquad (13a)$$

$$\bar{J}_{t:g,air} = \frac{1}{V_{air}}\int_0^{V_{air}} J_{t:g,air}\,dV \qquad (13b)$$

where $\bar{J}_{t:g,air}$ is the average (over axial position) $J_{t:g,air}$ and $\dot{V}_{E,ee}$ is $\dot{V}_E$ at end exhalation. Hence, an estimate of $C_{alv,ss}$ ($C_{alv,ee}$) is attained from the slope of a plot of E_{NO} vs. $\dot{V}_{E,ee}$. We used the elimination rate data from a representative subject (*subject 6*) in the companion article (26) for the model simulations. For *subject 6*, $C_{alv,ss}$ was equal to 8.11 parts/billion (ppb), and thus $\dot{S}_{app,alv}$ was estimated as 6.7×10^{-10} mol/s. $\dot{S}_{t,air}$ can also be estimated from *Eq. 13*, with the intercept of the E_{NO} vs. $\dot{V}_{E,ee}$ plot as an estimate of $\bar{J}_{t:g,air}A_{s,air}$. $\dot{S}_{t,air}$ is then chosen using an iterative scheme to satisfy *Eqs. 4* and *13* simultaneously, for which $\dot{S}_{t,air}$ is the only unknown parameter. In the case of *subject 6*, $\bar{J}_{t:g,air}A_{s,air}$ was equal to 2.33×10^{-11} mol/s, which produced a value for $\dot{S}_{t,air}$ of 5.5×10^{-13} mol · s^{-1} · cm^{-3}.

The model equations can be solved for different breathing patterns of constant $\dot{V}_E$ as well as $\dot{V}_E$ that change linearly in time (see APPENDICES C and D). The initial alveolar volume, inspired and expired volumes, and inspired and expired flow rates are specified by the user. Unless otherwise noted, inspiratory conditions for all simulations were from functional residual capacity to total lung capacity (alveolar volume 2,300 and 5,800 ml, respectively). Functional residual capacity and total lung capacity were estimated from the vital capacity (VC) of *subject 6* (9). The control inspiratory conditions also included the following parameter values: $\dot{V}_I = 2,000$ cm^3/s, $C_{alv,0} = 8.3$ ppb, and $C_I = 15$ ppb, where $C_{alv,0}$ is initial alveolar concentration and C_I is inspiratory concentration. $C_{alv,0}$ can be estimated by first setting its value to zero and then simulating several rebreathing maneuvers (tidal volume = 500 ml, respiratory rate = 12 breaths/min) by setting the initial concentration to the end-expiratory concentration of the previous maneuver. A steady-state value is quickly achieved, which can serve as $C_{alv,0}$ for the remaining simulations.

RESULTS

Simulation of the Single Exhalation

Figure 3 depicts four different experimental single-exhalation maneuvers of the representative subject (26) and the model prediction of these maneuvers with the same set of parameters (Table 1) in each case. Recall that no particular optimization procedure has been performed to simulate the experimental profiles. All parameters were estimated from the literature or from the elimination rate data from this particular subject. In Figure 3, *A* and *B*, the subject exhales at a constant low flow rate (control) and a constant high flow rate, respectively. In Fig. 3*C*, the control maneuver is performed after a 15-s breath hold, and in Fig. 3*D* $\dot{V}_E$

Table 1. *Parameter values for two-compartment model*

Parameter	Value	Units
Tissue		
$\lambda_{t:g}$	0.0416	mol/mol
D_t	3.3E-05	cm^2/s
k	0.173	s^{-1}
$L_{t,air}$	0.01	cm
$\dot{S}_{t,air}$	0.55	pmol · s^{-1} · cm^{-3}
Airway		
$A_{s,air}$	9,100	cm^2
V_{air}	200	cm^3
a_I	12	cm^{-1}
b_I	0.333	cm^2
Alveolar		
V_{alv}	2,300–5,800	cm^3
DL_{NO}	2,100	mol · s^{-1} · mol^{-1} · cm^3
$\dot{S}_{app,alv}$	670	pmol/s

$\lambda_{t:g}$, Partition coefficient of NO between tissue and air; D_t, molecular diffusion coefficient of NO in tissue; k, overall 1st order rate constant; $L_{t,air}$, thickness of tissue surrounding airway compartment; $\dot{S}_{t,air}$, rate of NO production by tissue in airway compartment; $A_{s,air}$, surface area of airway compartment; V_{air}, volume of airway compartment; a_I and b_I, constants for inspiration; V_{alv}, alveolar volume; DL_{NO}, diffusing capacity of NO in alveolar region; $\dot{S}_{app,alv}$, apparent production rate of NO in alveolar tissue.

Fig. 3. Model simulation (solid lines) of 4 different experimental exhalation NO profiles in which $\dot{V}_E$ is independent variable. *A*: control maneuver, which represents a constant $\dot{V}_E$ of ~200 cm³/s. *B*: high flow rate maneuver in which $\dot{V}_E$ is still constant but is increased to ~450 cm³/s. *C*: preexpiratory 15-s breath hold followed by a constant $\dot{V}_E$ of ~200 cm³/s. *D*: linear decrease of $\dot{V}_E$ in time during course of exhalation with a slope of approximately -40 cm³·s⁻¹·s and an average $\dot{V}_E$ of ~300 cm³/s. C_E, expiratory concentration; ppb, parts/billion.
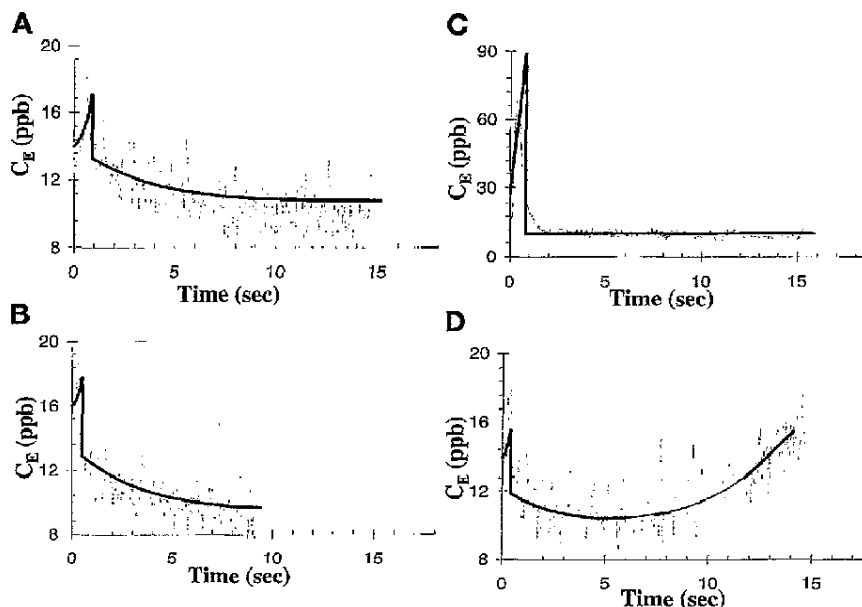
is decreasing linearly with time on the basis of the flow signal from this particular profile.

At a constant $\dot{V}_E$ (Fig. 3, *A* and *B*) the model replicates the initial rise in exhaled NO concentration (beginning at C_I) as the airway compartment is exhaled (first 200 ml or ~1 s). This rise represents an axial NO gradient due to the absorption of NO by the airstream from the airway tissue. After this initial peak, there is a step change as air from the alveolar compartment reaches the exhalate. This value (10 ppb) is larger than the steady-state alveolar concentration (8.11 ppb) and the initial or preexpiratory concentration (8.3 ppb) due to absorption of NO from the airway tissue as the airstream is convected through the airways. The model-predicted and experimental expiratory concentration (C_E) then steadily declines over the remaining portion of the exhalation. After a 15-s breath hold (Fig. 3*C*) the model predicts a large initial peak due to accumulation of NO in the airway compartment followed by a similar decline, although less pronounced, in C_E over the remaining exhalation. When $\dot{V}_E$ decreases linearly in time (Fig. 3*D*) the model is able to simulate the initial fall in C_E during phase III followed by a steadily increasing rise.

Flow Rate Dependence of the Average
Phase III Concentration

In Fig. 4, average phase III concentrations with respect to time [$\overline{C}_E(t)$] or volume [$\overline{C}_E(V)$] are plotted as a function of $\dot{V}_E$ over a wide range of constant $\dot{V}_E$. $\overline{C}_E(t)$ is estimated over a specified time interval (exhalation time of 2–8 s) and $\overline{C}_E(V)$ over a specified volume interval (exhalation volume of 20–60% of VC), as described in the companion article (26). For

very low or very high $\dot{V}_E$, where phase III does not include the above intervals, the maximum allowable interval is used. The experimental data from the companion article are also reported for reference. There is a good agreement between our experimental data and our simulations for intermediate flow rates. Over the entire flow rate range there is an exponential decrease for $\overline{C}_E(t)$ and $\overline{C}_E(V)$ with $\dot{V}_E$. This result is consistent with the experimental data (end-exhaled NO concentration) presented by Silkoff et al. (24) over the range 4.2–1,500 cm³/s. For low $\dot{V}_E$ (<500 cm³/s), $\overline{C}_E(t)$ has a slightly larger value. In the high-$\dot{V}_E$ region (>500 cm³/s), $\overline{C}_E(V)$ is slightly higher and has a small positive slope. In the intermediate region the slope of $\overline{C}_E(t)$ vs. flow (-0.004 ppb·ml⁻¹·s⁻¹) is steeper than for $\overline{C}_E(V)$ (-0.002 ppb·ml⁻¹·s⁻¹), which is in agreement with our experimental data (see Fig. 4 in Ref. 26).
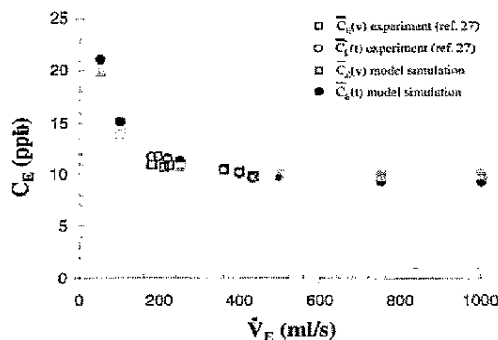

Fig. 4. Dependence of average NO concentration in phase III ($\overline{C}_E$) with respect to time (*t*) and volume (*V*) over a wide range of $\dot{V}_E$.

Phase III Slope

Figure 5 presents data from the simulation of linearly changing flow rate profiles. The normalized phase III slope (slope in phase III normalized by the average concentration in phase III) in time $[\overline{S}_{III,NO}(t)]$, is plotted as a function of the normalized slope of V_E $[\overline{S}_{III,\dot{V}_E}(t)$; see Fig. 6 of Ref. 26]. To generate the data, the model simulated the exhalation maneuvers of *subject 6*, matching the experimental flow rate profile of each maneuver. The simulations are performed for the breath-hold and the non-breath-hold maneuvers. The experimental data for *subject 6* are also shown for comparison. The model is able to simulate the inverse relationship, including the negative intercept at a constant V_E. The inverse relationship is due to the nonnegligible contribution from the airways to exhaled NO and, hence, the flow rate dependence. As V_E decreases, C_E increases. Thus, if V_E decreases in time, C_E will increase in time and affect the slope of phase III. The slight negative slope at constant V_E is generated from continuous gas exchange in the alveolar region. In addition, in a fashion similar to the experimental data, the intercept increases after a 15-s breath hold. This phenomenon is due to a decrease in the alveolar concentration toward the steady-state value during the 15-s breath hold (see *Inspiratory Conditions*).

Elimination Rate

In Fig. 6 we present E_{NO} at the end of expiration, estimated as the product of end-expiratory exhaled concentration and V_E. The data are derived from model simulations of constant V_E (range 50–1,000 cm³/s) exhalation maneuvers with or without a 15-s breath hold. For $V_E > 500$ ml/s only data from the breath-hold experiments were used to ensure an elapsed time of ≥ 8 s from end inspiration (see *Inspiratory Conditions*). Least squares linear regression over the resulting data reveals a highly linear ($R^2 = 0.99$) dependence of E_{NO} with V_E. The slope and intercept of the linear regres-
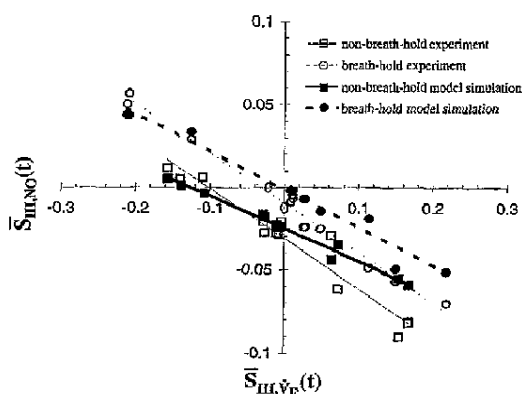
Fig. 5. Experimental and model-predicted relationship between normalized phase III slope of exhaled NO concentration in time $[\overline{S}_{III,NO}(t)]$ and exhalation flow rate $[\overline{S}_{III,\dot{V}_E}(t)]$ with and without a 15-s breath hold.
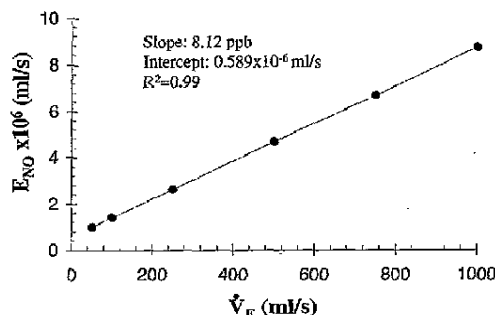
Fig. 6. Model-predicted relationship between elimination rate of NO at end exhalation (E_{NO}) and V_E. E_{NO} is defined as product of end-exhaled concentration and V_E. Positive slope is consistent with a nonzero alveolar concentration of NO; nonzero intercept is consistent with a nonnegligible flux of NO from airway tissue.

sion line are 8.12 ppb and 0.589×10^{-6} ml/s, respectively, which are in close agreement with the experimental values from *subject 6* (8.11 ppb and 0.592×10^{-6} ml/s). The nonzero slope and intercept are due to significant contributions of exhaled NO from the expansile alveoli and the nonexpansile airways (*Eq. 13*).

Inspiratory Conditions

In Fig. 7 the model-predicted effect of the inspired conditions on the exhalation profile of NO is examined. Although this represents an extrapolation of the model, this type of prediction can be used to guide future experimentation. Figure 7A presents the model's prediction for the NO single-exhalation profile. Three different values for the inhaled concentration are shown: 0, 15, and 30 ppb. For $C_I = 0$ the model predicts an initial rise from 0 ppb as the conducting airway space is emptied, then a more gradual rise to the same plateau value seen previously for $C_I = 15$ ppb. The result is a positive slope for phase III. In addition, the model predicts obliteration of the peak in phase I after inspiration of NO-free air. For $C_I = 30$ ppb, there is, again, an initial rise in C_E as the airway compartment is emptied, which is then followed by a steeper decline to the end-exhalation value compared with $C_I = 15$ ppb. Hence, the model predicts that ambient concentration can significantly affect the peak and the slope of phase III during exhalation.

Figure 7B presents the effect of $\dot{V}_I$ on the exhalation profile when V_I, C_I, and V_E are held constant at the control values ($C_I = 15$ ppb, $\dot{V}_E = 250$ cm³/s, $V_I = 3,500$ ml). The model predicts that the slope of phase III becomes progressively smaller as $\dot{V}_I$ decreases from 2,000 to 100 cm³/s, yet the end-exhalation concentration remains unchanged. In addition, $\dot{V}_I$ affects the peak in phase I; the maneuver of the slowest $\dot{V}_I$ produces the highest peak.

Figure 7C presents the effect of V_I on the exhalation profile. The model predicts that only the slope of phase III becomes progressively larger as V_I decreases from
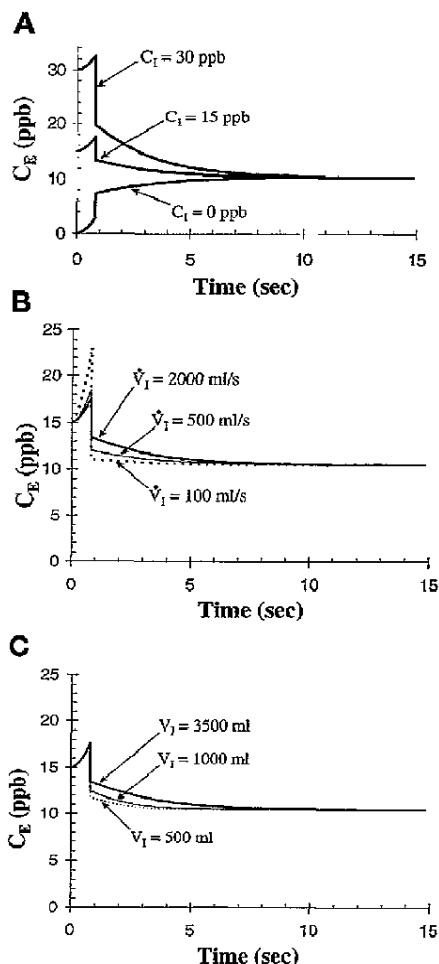
Fig. 7. Effect of inspired conditions (flow rate, volume, and concentration) on shape of exhalation profile and alveolar concentration. *A*: exhalation profile at 3 different C_I. *B*: exhalation profile at 3 different $\dot{V}_I$. *C*: exhalation profile at 3 different V_I.

Fig. 8. Alveolar concentration at end inspiration ($C_{alv,ei}$) as a function of C_I and $\dot{V}_I$.

Fig. 9. Model-predicted steady-state radial concentration profile in airway tissue as a function of C_I. *A*: low concentrations [$0 < C_I < 1$ part/million (ppm)]. *B*: high concentrations ($C_I = 50$ or 100 ppm).

3,500 to 500 cm³, while the peak in phase I remains unaffected.

The above results can be understood by examining the alveolar concentration of NO under these conditions. Figure 8 demonstrates the alveolar concentration of NO at end inspiration ($C_{alv,ei}$) under different conditions of C_I and $\dot{V}_I$. $C_{alv,ss}$ is 8.11 ppb. For C_I in excess of ~5 ppb, there is an increase in $C_{alv,ei}$ above $C_{alv,ss}$. Hence, during exhalation there is a net negative flux of NO (e.g., toward the pulmonary blood) in the alveolar compartment as $DL_{NO}C_{alv} > S_{app,alv}$ (*Eq. 9*). The result is a progressively decreasing C_{alv}, and hence C_E, during exhalation until C_{alv} reaches $C_{alv,ss}$. At this point, C_E reaches a plateau value of 10 ppb (for the control V_E). The opposite scenario occurs for C_I less than ~5 ppb. Under these conditions, $C_{alv,ei}$ is below $C_{alv,ss}$, and $DL_{NO}C_{alv} < S_{app,alv}$. The result is an exponential rise in

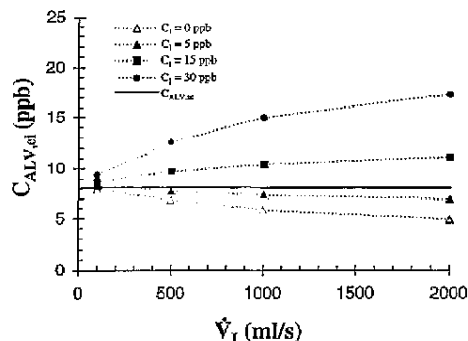C_{alv} and C_E during exhalation. The time constant for this exponential decline or rise is equal to $V_{alv}(t)/DL_{NO}$ or ~1–3 s over the course of exhalation. Thus the model predicts that an exhalation time of ~8 s will achieve an alveolar concentration that differs by <1% of the steady-state concentration. In addition, the difference between $C_{alv,ei}$ and $C_{alv,ss}$ for any given inspired concentration is increased with $\dot{V}_I$. As a result, phase III slope is also affected by $\dot{V}_I$ (Fig. 7*B*).

Concentration Profile in the Airway Tissue

The steady-state concentration profile in the airway tissue, as predicted by the model, for different inhaled NO concentrations is shown in Fig. 9. The radial distance (*x*) is considered zero at the blood-tissue interface. For C_I less than ~418 ppb (derived from zero net flux or the ratio a/b from *Eq. 4*), which is usually the case for inspiration of ambient air, there is a net
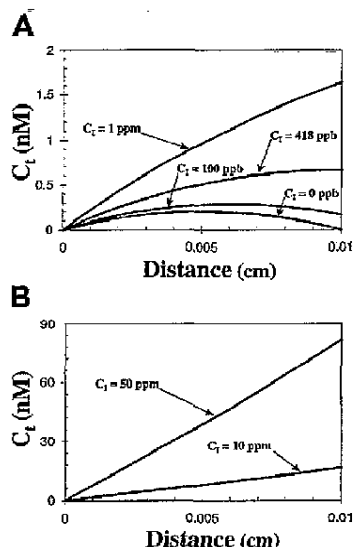
positive flux of NO or absorption of NO by the airstream. For C_I greater than ~418 ppb (i.e., when exogenous NO is inspired for clinical application), the net flux of NO is negative, or there is desorption of NO from the airstream to the airway tissue. At these higher concentrations the tissue concentration profile is approximately linear when $t_{1/2}$ is 4 s. Under these circumstances, the consumption rate of NO within the tissue is small compared with the flux of NO from the airstream.

Exogenous NO

In Fig. 10*A* we present the model predictions for the fate of exogenous NO at concentrations that are representative of clinical situations [C_I = 10 parts/million (ppm)]. A single rebreathing maneuver of the tidal volume (V_I = 500 ml) is simulated, while $\dot{V}_I$ and $\dot{V}_E$ are held constant ($\dot{V}_I$ and $\dot{V}_E$ = 250 ml/s). The model predicts that 55.1% of inspired NO (90% of the NO that actually reaches the alveoli) is absorbed by the pulmonary blood in the alveoli. In contrast, only a very small portion (0.4%) of the inspired NO is absorbed by the airway. The remaining 44.5% of inspired NO is exhaled.

In Fig. 10, *B* and *C*, the percentage of NO absorbed by the airway tissue is calculated under different conditions. In Fig. 10*B*, C_I and flow rate change from 10 to 100 ppm and from 50 to 1,000 ml/s, respectively. In Fig. 10*C*, simulations are performed twice, with and with-
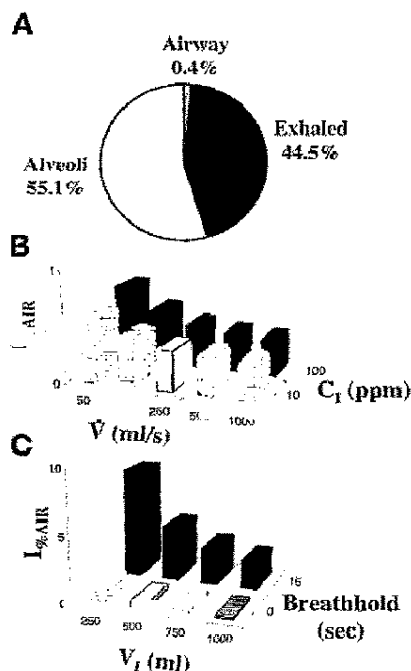

Fig. 10. *A*: distribution of absorbed inhaled exogenous NO (C_I = 10 ppm) between alveoli and airway compartments for tidal breathing. *B*: effect of flow rate and inspiratory concentration on the percent NO absorbed by airway tissue ($I_{\%,air}$). *C*: effect of inspiratory volume and breath-hold time on $I_{\%,air}$.
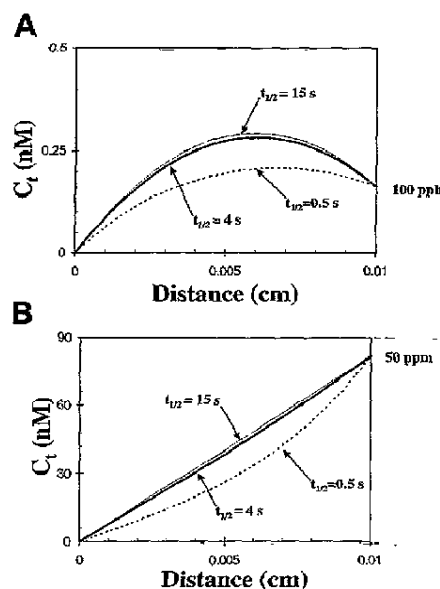

Fig. 11. Effect of reaction rate [or half-life ($t_{1/2}$)] on radial tissue concentration profile for 2 different gas phase concentrations: 100 ppb (*A*) and 50 ppm (*B*).

out a 15-s breath hold, with different inspired volumes (V_I = 250–1,000 ml). The percentage of inspired NO absorbed by the airway tissue ($I_{\%,air}$) is inversely related to $\dot{V}_E$, $\dot{V}_I$, and V_I and is a positive function of breath-hold time and C_I. Maximum absorption (8% of total NO inspired) in the airway tissue occurs when residence time in the airway compartment is maximized and contact with the alveolar compartment is minimized: V_I of 250 ml and 15-s breath hold.

Reaction Rate Constant in Tissue

To investigate the sensitivity of the exhalation profile on the reaction kinetics in the tissue, we varied $t_{1/2}$ between 0.5 and 15 s, which corresponds to a range in k from 1.38 to 0.046 s^{-1}. Figure 11 demonstrates that $t_{1/2}$ values <4 s affect significantly the tissue concentration profile. Decreasing $t_{1/2}$ corresponds to a higher k or more rapid consumption of NO. The result is a reduced average concentration of NO in the tissue and an increased radial gradient at the airway wall. For low ($C_I \ll 418$ ppb) inspired concentrations, the flux from the tissue to the airway is reduced. For high ($C_I \gg 418$ ppb) concentrations, the flux to the tissue from the airstream increases.

DISCUSSION

Model Validation

The model is able to simulate the different single-exhalation maneuvers (Fig. 3) extremely well. This finding becomes even more significant if one considers that only rough approximations of critical parameters were used (DL_{NO}, $S_{app,alv}$, and $S_{t,air}$) that were acquired

by independent means. No adjustment of model parameters was made to optimize the model prediction of the experimental exhalation profile. The data are presented for only a representative subject, inasmuch as our goal was only to simulate the fundamental features of the exhalation profile under dynamically changing conditions. The small differences between the experimental profiles and the simulations can be attributed to model simplifications and parameter estimation.

The model assumes that the lung consists of two well-defined, separate regions: a rigid airway compartment and a well-mixed, expansile alveolar compartment. Such a division represents an idealization of the actual lungs. For example, the volume of the airways has been shown to change during breathing, there is a transitional region (respiratory bronchioles) between the airways and the alveolar region, and there may be axial concentration gradients within the alveolar region (22). Although our model does not consider these features, the error introduced is minimal in relation to the model's ability to describe the basic features of NO exchange.

The model appears to fail to predict the exact value of the initial peak (phase I) in an inconsistent fashion. The peak is underestimated in Fig. 3, A, B, and D, and overestimated in the breath-hold maneuver (Fig. 3C). Because our model does not include axial diffusion, one would expect the predicted peaks to be overestimated. Axial dispersion and mixing, especially at the interface between the alveolar and the airway regions, would create a broader peak width and hence a smaller peak height. The underestimation of the peak in Fig. 3, A, B, and D, is an artifact that arises from the fact that the model simulates a step change for the flow, from inspiration to expiration, while in reality a small period of decreasing V_I or zero flow might have occurred. In fact, a small breath-hold time (~0.5 s) between inspiration and expiration may represent more accurately a single-exhalation maneuver and will increase the height of the peak in phase I.

The model's simulation of phase III under the wide range of flow conditions is quite reasonable. Although we measured the average concentration in phase III experimentally over only a small range of flow rates, there is good agreement (Fig. 4). In addition, over a wider range of flow rates, the model is able to predict the same functional dependence reported by Silkoff et al. (24).

The phase III slope under constant-flow conditions and under dynamically changing flow conditions is similar to the experimental data (Fig. 5), but several important differences exist. First, the intercept (phase III slope at constant V_E) is larger for the experimental data and importantly the model predicts a zero intercept after a 15-s breath hold. Second, the slope of $\overline{S}_{III,NO}(t)$ vs. $\overline{S}_{III,\dot{V}_E}(t)$ is steeper for the experimental data with and without a 15-s breath hold. Both of these discrepancies are likely due to simplifications in the model structure or parameter estimation.

The model predicts a zero intercept after a breath hold simply because a period of 15 s is long enough for C_{alv} to reach its steady-state value (as discussed previously). The structure of the model only allows for two mechanisms to create a phase III slope: *1*) continuing gas exchange and *2*) nonconstant absorption from the airway tissue. Continuing gas exchange is eliminated if C_{alv} reaches $C_{alv,ss}$, and the model predicts that, under ambient or physiological conditions (C_I less than ~50 ppb), the absorption of NO from the airway tissue is essentially constant. Hence, the presence of a nonzero intercept experimentally after a 15-s breath hold is evidence that there are other mechanisms affecting gas exchange that cannot be completely neglected. For example, inhomogeneity in alveolar concentrations due to heterogeneous distributions of ventilation-to-volume ratios has been shown to contribute to the positive phase III slope of gases with similar physical characteristics (18, 19). In addition, axial or serial heterogeneity in the concentration of the gas in the respiratory region (respiratory bronchioles through the terminal alveoli) has been shown to contribute to the phase III slope of CO_2, SF_6, and He (22). The current model, of course, assumes a well-mixed alveolar compartment of uniform concentration that empties through a single path. The model also neglects axial diffusion, which may serve to increase C_{alv} above its steady-state value during a breath-hold maneuver.

Regarding the slope of $\overline{S}_{III,NO}(t)$ vs. $\overline{S}_{III,\dot{V}_E}(t)$, a number of possible reasons can justify the small difference with the experimental data. DL_{NO} has been demonstrated experimentally to be a positive function of lung volume (3). This contrasts with CO and is due to the relatively rapid kinetics of NO with hemoglobin. The rapid kinetics create a greater dependence of DL_{NO} with surface area available for diffusion. The model assumes a constant DL_{NO} throughout the exhalation. In addition, DL_{NO} varies among subjects. The value of DL_{NO} for *subject 6* may be different from the mean value from Borland et al. (3) used in the simulations. The value of DL_{NO} can affect the phase III slope by affecting the rate at which C_{alv} approaches $C_{alv,ss}$ [time constant is equal to $V_{alv}(t)/DL_{NO}$]. Inspiratory conditions affect the phase III slope (Fig. 7), and they were not controlled during the experiments. Finally, the phase III slope is curvilinear. Hence, the magnitude of $\overline{S}_{III,NO}(t)$ is highly dependent on the interval of linear regression.

A final point to consider related to the dependence of phase III on a changing flow rate is the relative magnitude of NO production in the airway and alveolar tissue. There is great intersubject variability in the slope and intercept of the experimental data of E_{NO} vs. V_E (Fig. 7 of Ref. 26); hence, there appears to be great variability in the relative ratio of NO production in the airway tissue to that in the alveolar tissue. For *subject 1*, $C_{alv,ss}$ is very small, yet the intercept is similar to that of *subject 6*. This is consistent with a larger relative rate of NO production in the airway tissue; hence, this subject demonstrates a steeper slope of $\overline{S}_{III,NO}(t)$ vs. $\overline{S}_{III,\dot{V}_E}(t)$ (Fig. 6 in Ref. 26). In the model simulations, values for $S_{app,alv}$ and $\dot{S}_{t,air}$ were chosen for a representative subject but are only approximations. A small underestimation of $\dot{S}_{t,air}$ relative to $S_{app,alv}$ can generate

a smaller slope in the $\overline{S}_{III,NO}(t)$ vs. $\overline{S}_{III,\dot{V}_E}(t)$ diagram (i.e., less dependence of exhaled NO on the flow rate).

Elimination Rate

The positive dependence of E_{NO} vs. $\dot{V}_E$ has been experimentally reported (20, 24, 26). Silkof et al. (24), in agreement with our experimental findings (26), demonstrated a linear relationship between $\dot{V}_E$ and E_{NO} at the end of a single constant $\dot{V}_E$. In addition, we observed a similar dependence of E_{NO} in single exhalations with a dynamically changing $\dot{V}_E$. The model proposed by Hyde et al. (11) predicted an increase in E_{NO} with increasing ventilatory rate. With the assumption of constant lung volume, a steady-state approximation, and inspiration of NO-free air, they demonstrated an increase in E_{NO} when the rate of ventilation was increased. Higher ventilatory rates resulted in a lower NO concentration in the lung, and thus the uptake of endogenously produced NO is shifted from absorption by the pulmonary blood to elimination by the exhaled breath. The above conclusion can satisfactorily describe a maneuver that has reached a periodic steady state (i.e., a steady-state rebreathing maneuver of NO-free air); however, this conclusion cannot be used to directly describe a single exhalation where the lung volume and concentration of NO are changing in time.

Our model demonstrates that a nonzero alveolar concentration can satisfactorily describe the positive dependence of E_{NO} on $\dot{V}_E$. At the end of exhalation the alveolar concentration, which is independent of $\dot{V}_E$ (expansile nature of alveoli, see *Eq. 10*), approaches a steady-state value; thus the positive dependence between E_{NO} and $\dot{V}_E$ becomes highly linear (*Eq. 13a*). However, there are at least two different possible explanations for the same phenomenon. First, Silkoff et al. (24) argued that at high flow rates the NO concentration in the bulk gas will decrease, thus maximizing the gradient and the flux between the airway wall and the gas. Such an explanation is valid only if the transport of NO from the site of production to the bulk gas is limited by diffusion through the gas phase. Examination of the gas phase resistance along the airway (APPENDIX B) strongly suggests that, because of the very low solubility of NO, resistance to diffusion in the gas phase is very small compared with diffusion in the tissue (6). Second, we suggested previously (26) that high flow rates would result in lower gas-phase and tissue-phase concentrations of NO and, hence, lower consumption by first-order chemical reactions and a larger flux of NO into the gas phase. However, the model demonstrates that first-order consumption of NO has only a minimal impact on the flux of NO at the airway wall. For example, if $\dot{V}_E$ changes from 200 to 400 ml/s in *subject 6*, E_{NO} increases by 75% (Fig. 6). However, <1% of the change in E_{NO} can be attributed to a decreased consumption in the tissue, even at the extreme $t_{1/2}$ of 0.5 s. The model's ability to recreate the experimental relationship of E_{NO} to $\dot{V}_E$ suggests that an experimental plot of E_{NO} vs. $\dot{V}_E$ is an acceptable method of determining the relative contribution of the alveolar tissue and airway tissue to exhaled NO. This has important implications for using exhaled NO as a noninvasive index of regional lung inflammation. For example, assessing airway inflammation in bronchial asthma might be accomplished by examining the magnitude of the peak in phase I. The main disadvantage of this technique is the difficulty in attaining a reproducible signal considering the short exhaled volume that is involved and the effect of ambient levels of NO on the magnitude of this peak. E_{NO} at end exhalation uses only the steady-state concentration of exhaled NO, which is independent of inspiratory conditions, yet when plotted against $\dot{V}_E$ gives an accurate assessment of the relative production rates of NO in the airways and the alveoli. For example, we might anticipate an individual with active bronchial asthma to have a larger intercept (larger airway production) than normal (or compared with a previous test by the same subject before active inflammation) but the same slope. In contrast, an individual with pneumonia would have an increase in the slope but no change in the intercept.

Exercise and hyperventilation have been demonstrated to increase E_{NO}, but the mechanism is unknown (1, 17, 20, 21, 25). Theories have included an increased production rate by the endothelial cells due to increased shear rate by the blood (17) and an increased DL_{NO} (11). Our simple model suggests that the increased ventilatory rate associated with a nonzero C_{alv} can explain a large portion of the experimental observations. The increased DL_{NO} that is associated with exercise (4) cannot be used to explain the increased elimination, as suggested by Hyde et al. (11). In fact, an increased DL_{NO} serves to decrease C_{alv} (*Eq. 12*) and would thus tend to decrease E_{NO}. E_{NO} increases in response to exercise, because the increase in DL_{NO} does not lower C_{alv} enough to compensate for the increase in the ventilatory rate.

Inspiratory Conditions

Initial reports have suggested that ambient levels of NO do not affect the exhalation profile. Our model predicts that the NO exhalation profile, in particular the early part of phase III, is affected by not only the inspired concentration of NO, but also V_I and $\dot{V}_I$. An interesting finding is the comparison of the peak values in phase I under the different inspiratory conditions. Inspiration of NO-free air obliterates the early peak of phase I in the absence of a breath hold. Similar experimental findings have been reported by Silkoff et al. (24), who reported no early peak when subjects inspired NO-free air. The absence of the phase I peak in these conditions does not indicate a lack of accumulation of NO in the airway, only that the accumulation leads to a concentration below C_{alv}. The model predictions related to inspiratory conditions provide a strong impetus and direction for further experimentation on the factors that control the NO exhalation profile.

Exogenous NO

Only a small amount (0.3–8%) of inspired exogenous NO at clinically relevant concentrations is absorbed by

the airway tissue. By use of a $t_{1/2}$ of 4 s, >90% of the NO that is absorbed by airway tissue is then absorbed by hemoglobin in bronchial circulation. This is evident by the relatively linear concentration profile of NO in the tissue layer at high C_I. For a linear profile, the gradient (dC_t/dx) at the interface of the blood and tissue is the same as at the interface of the tissue and airstream; hence, the fluxes are the same. This model prediction depends on the value of the reaction rate constant, which may be underestimated at high tissue concentrations when reactions with O_2 and thiols (2nd order in NO concentration) can no longer be neglected (2). In addition, the bronchial circulation is truly represented in vivo by discrete capillaries embedded with the tissue layer. Hence, some exogenous NO may diffuse through the tissue and reach important tissue layers such as the bronchial smooth muscle. Nonetheless, the current model provides an explanation for why exogenous NO has only a mild bronchodilator effect in humans (10): most of the exogenous NO that is inhaled is absorbed by the pulmonary circulation or is exhaled, and that which is absorbed by the airway tissue is primarily absorbed by the bronchial circulation before reaching the bronchial smooth muscle. Furthermore, because a steady state in the tissue is reached in <1 s, the model predicts that the concentration of NO in the tissue depends only on C_I and not on rate of absorption.

Conclusion

A relatively simple and robust two-compartment model of NO has been developed that is capable of simulating many important features of NO exchange in the lungs. The model is able to simulate the experimentally observed dependence of exhaled NO concentration (and hence the dependence of the phase III slope and the elimination rate) on V_E. This result stems from a nonnegligible contribution of NO in the exhaled breath from the expansile alveoli and the nonexpansile airways. The model predicts that continuing gas exchange in the alveoli can explain a large part of the phase III dynamics of NO. However, additional important parameters that can influence the shape of the NO exhalation profile include preexpiratory breath hold, $\dot{V}_I$, V_I, and inspiratory NO concentration. The effect of inspiratory conditions on the exhalation profile has not been well studied experimentally but may play a critical role in the the interpretation of the NO exhalation profile. However, the model also predicts that the alveolar concentration approaches its steady-state value if exhalation is ≥8 s long. Thus the expiratory concentration is independent of inspiratory conditions if duration of exhalation is greater than ~8 s. Finally, the model suggests that the relationship between $\dot{E}_{NO}$ at end-exhalation (exhalation time > 8 s) and $\dot{V}_E$ may be a simple, effective, and reproducible technique for determining the relative contribution of the airways and alveoli to exhaled NO.

APPENDIX A

The unsteady diffusion equation for the tissue compartment (*Eq. 1*) is solved for the simplified case of a steady state

(*Eq. 3*). To justify this assumption, the unsteady equation must be solved and analyzed. If the gas phase concentration suddenly increases from 0 to a constant value C_I (i.e., inspired concentration), the concentration profile of NO in the tissue will be given from the solution of *Eq. 1* with the following boundary conditions

$$C_t(t, 0) = 0 \qquad (A1a)$$

$$C_t(t, L_{t,air}) = C_W = C_I/\lambda_{t:g} \qquad (A1b)$$

The initial condition is derived from *Eq. 3* for $C_W = 0$

$$C_t(0, x) = \alpha_1 \frac{\dot{S}_{t,air}}{k} e^{x/\beta} - \alpha_2 \frac{\dot{S}_{t,air}}{k} e^{-x/\beta} + \frac{\dot{S}_{t,air}}{k} \qquad (A1c)$$

where

$$\alpha_1 = \frac{-1 + e^{-L_{t,air}/\beta}}{e^{L_{t,air}/\beta} - e^{-L_{t,air}/\beta}}, \qquad \alpha_2 = \alpha_1 + 1$$

In dimensionless form, *Eq. 1* can be written as follows

$$\frac{\partial^2 \Theta}{\partial z^2} - \mu^2 \Theta = \frac{\partial \Theta}{\partial \tau} \qquad (A2a)$$

with

$$\Theta(0, z) = \alpha_1 e^{\mu z} - \alpha_2 e^{-\mu z} \qquad (A2b)$$

$$\Theta(\tau, 0) = -1 \qquad (A2c)$$

$$\Theta(\tau, 1) = \frac{C_W - \dot{S}_{t,air}/k}{\dot{S}_{t,air}/k} = \zeta \qquad (A2d)$$

where

$$\Theta = \frac{C_t - \dot{S}_{t,air}/k}{\dot{S}_{t,air}/k}, \quad z = \frac{x}{L_{t,air}}, \quad \tau = \frac{t}{L_{t,air}^2/D_t}, \quad \mu = L_{t,air}\bigg/\sqrt{\frac{D_t}{k}}$$

By use of the method of separation of variables, *Eq. A2* can be solved to give the following solution

$$\Theta = \sum_{n=1}^{\infty} \frac{2n\pi}{\mu^2 + n^2\pi^2} (e^{-n^2\pi^2\tau} - e^{\mu^2\tau}) \sin(n\pi z)$$

$$+ \sum_{n=1}^{\infty} \frac{2n\pi\zeta}{\mu^2 + n^2\pi^2} (e^{-n^2\pi^2\tau} - e^{\mu^2\tau}) \sin[n\pi(1-z)] \qquad (A3)$$

$$+ \sum_{n=1}^{\infty} \frac{2n\pi[(-1)^n - 1]}{\mu^2 + n^2\pi^2} e^{-n^2\pi^2\tau} \sin(n\pi z)$$

In Fig. 12 the solution of the dimensionless concentration (Θ) is plotted as a function of the dimensionless radial distance (z) for different values of the dimensionless time (τ). The profiles computed from *Eq. A3* for $\mu^2 = 0.524$ and $\zeta = -0.97$ correspond to a tissue thickness of 100 μm and a step change in the gas concentration of NO from 0 to ~60 ppb, respectively. One can see that at $\tau = 0.2$ ($t = 0.6$ s) the concentration of NO at any given point in the tissue is within 10% of the steady-state value. As a result, under normal conditions (i.e., inspiration of room air of small NO concentration and expiration time >2 s) the error introduced by the steady-state
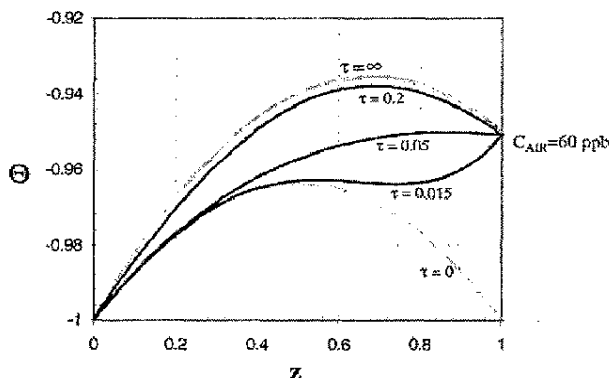
Fig. 12. Effect of a step change in gas-phase concentration on radial tissue concentration profile from 0 to 60 ppb.

assumption is negligible. However, for a fast breathing maneuver of a concentrated gas mixture of NO, such an assumption is not valid.

APPENDIX B

The radial gas phase resistance for the diffusion of NO is negligible and can be proven using the following argument: If there is a significant gas phase resistance in the transport of NO between the tissue and the bulk gas, then *Eq. 4* can be rewritten as

$$J_{t:g,air} = a - bC_W = K_s(C_W/\lambda_{t:g} - C_{air}) \qquad (B1)$$

and solving for C_W

$$C_W = \frac{a + K_s C_{air}}{b + K_s/\lambda_{t:g}} \qquad (B2)$$

where K_s is the gas phase mass transfer coefficient for NO, $\lambda_{t:g}$ is the partition coefficient between the liquid and the gas phase, C_{air} is the the concentration of NO in the bulk gas, and a and b are constants from *Eq. 4*.

The Sherwood number ($Sh = K_s d_{air}/D_{gas}$) in the airway tree, although dependent on the flow rate and the axial position, has values usually between 6 and 10 (6). The diffusivity of NO in the gas phase (D_{gas}) is 0.23 cm²/s, and the diameter of the airway tree (d_{air}) is between 2 cm and 5 mm. Thus, even under the extreme conditions, K_s has a minimum value of 0.69 cm/s. The values for the constants a and b, as estimated for the typical subject of our simulations, are 0.067 ppb·cm^{-1}·s^{-1} and 0.0039 cm/s, respectively. Because $(K_s/\lambda_{t:g}) \gg b$ and $(a/K_s) \ll C_{air}$, *Eq. B2* can be written as

$$C_W \approx \lambda_{t:g} C_{air} \qquad (B3)$$

Hence, the NO exchange between the tissue and the airway is not gas-phase diffusion limited.

APPENDIX C

Solution for the mass balance of NO in the alveolar compartment (*Eq. 10*) can be easily derived for a simple case of linearly time-dependent V_E. For an initial flow rate and slope ($\dot{V}_{E,0}$ and s, respectively)

$$\dot{V}_E(t) = \dot{V}_{E,0} + st \qquad (C1)$$

From *Eq. C1*

$$V_{alv}(t) = V_{alv}(0) - \dot{V}_{E,0}t - st^2/2 \qquad (C2)$$

Then, the solution to *Eq. 10* will be, for *case I*, for $\Delta = \dot{V}_{E,0}^2 + 4sV_{alv}(0) > 0$ (always true when the flow rate is increasing)

$$C_{alv}(t) = \frac{\dot{S}_{app,alv}}{DL_{NO}}$$
$$+ \left[C_{alv}(0) - \frac{\dot{S}_{app,alv}}{DL_{NO}}\right] e^{-[2DL_{NO}Tanh^{-1}[(\dot{V}_{E,0}+2st)/\sqrt{\Delta}]/\sqrt{\Delta}]} \qquad (C3a)$$

$$= \frac{\dot{S}_{app,alv}}{DL_{NO}} + \left[C_{alv}(0) - \frac{\dot{S}_{app,alv}}{DL_{NO}}\right]\left|\frac{t - t_1}{t - t_2}\right|^{-(DL_{NO}/\sqrt{\Delta})}$$

where

$$t_{1,2} = \frac{-\dot{V}_{E,0} \pm \sqrt{\Delta}}{2s}$$

for *case II*, for

$$\Delta = \dot{V}_{E,0}^2 + 4sV_{alv}(0) < 0$$

$$\left[\text{decreasing flow rates with } |s| > \frac{\dot{V}_{E,0}^2}{4V_{alv}(0)}\right]$$

$$C_{alv}(t) = \frac{\dot{S}_{app,alv}}{DL_{NO}}$$

$$+ \left[C_{alv}(0) - \frac{\dot{S}_{app,alv}}{DL_{NO}}\right] e^{-[2(DL_{NO})Tan^{-1}[(-\dot{V}_{E,0}-2st)/\sqrt{|\Delta|}]/\sqrt{|\Delta|}]} \qquad (C3b)$$

APPENDIX D

The mass balance in the upper airway compartment can also be solved for nonconstant flow rates. For the simple case of a linearly changing $\dot{V}_E$ and A_s/A_c, a linear function of V, *Eq. 6* becomes

$$-(\dot{V}_{E,0} + st)\frac{\partial C_{air}}{\partial V} + (a - bC_{air})(a_E + b_E V) = \frac{\partial C_{air}}{\partial t} \qquad (D1a)$$

with the general initial and boundary conditions

$$C_{air,(t=0)} = f(V) \qquad (D1b)$$

$$C_{air,(V=0)} = g(t) \qquad (D1c)$$

In dimensionless form, *Eq. D1* can be written as

$$\frac{\partial \Xi}{\partial \tau} + (2 + 2\tau)\frac{\partial \Xi}{\partial z} = -(c + dz)\Xi \qquad (D2a)$$

$$\Xi(0, z) = \frac{f\left(\frac{\dot{V}_{E,0}^2}{2s}z\right) - a/(b\lambda_{t:g})}{\dot{V}_{E,0}/s} \qquad (D2b)$$

$$\Xi(\tau, 0) = \frac{g\left(\frac{\dot{V}_{E,0}}{s}\tau\right) - a/(b\lambda_{t:g})}{\dot{V}_{E,0}/s} \qquad (D2c)$$

where

$$\Xi = \frac{C_{air} - a/b\lambda_{t:g}}{\dot{V}_{E,0}/s}, \quad \tau = \frac{t}{\dot{V}_{E,0}/s}, \quad z = \frac{V}{\dot{V}_{E,0}^2/(2s)},$$

$$c = \frac{b\dot{V}_{E,0}}{s}a_E, \quad d = \frac{b\dot{V}_{E,0}^3 b_E}{2s^2}$$

Eq. D2 can be solved using the method of characteristics to obtain *region I* for $(\tau + 1)^2 - 1 < z$

$$\Xi(t, z) = \frac{f\{-[\dot{V}_{E,0}^2/(2s)]u\} - a/(b\lambda_{t:g})}{\dot{V}_{E,0}/s}e^{-c\tau+d\tau(\frac{3}{2}\tau^2+\tau-z)} \quad (D3a)$$

region II for $(\tau + 1)^2 - 1 > z$

$$\Xi(t, z) = \frac{g[\dot{V}_{E,0}/s(\sqrt{u + 1} - 1)] - a/(b\lambda_{t:g})}{\dot{V}_{E,0}/s}$$

$$\times e^{d\sqrt{u+1}-1-\tau|+\frac{1}{2}dA} \quad (D3b)$$

with

$$u = (t + 1)^2 - 1 - z$$

$$A = \frac{1}{2}(\sqrt{u + 1} - 1)^2 - u(\sqrt{u + 1} - 1) + \tau u - \frac{1}{2}\tau(\tau + z)$$

REFERENCES

1. Bauer, J. A., J. A. Wald, S. Doran, and D. Soda. Endogenous nitric oxide in expired air: effects of acute exercise in humans. *Life Sci.* 55: 1903–1909, 1994.
2. Beckman, J. S., and W. H. Koppenol. Nitric oxide, superoxide, and peroxynitrate: the good, the bad, and the ugly. *Am. J. Physiol.* 271 *(Cell Physiol.* 40): C1424–C1437, 1996.
3. Borland, C. D. R., and T. W. Higenbottam. A simultaneous single breath measurement of pulmonary diffusing capacity with nitric oxide and carbon monoxide. *Eur. Respir. J.* 2: 56–63, 1989.
4. Ceretelli, P., and P. I. DiPrampero. Gas exchange in exercise. In: *Handbook of Physiology. The Respiratory System. Gas Exchange.* Bethesda, MD: Am. Physiol. Soc., 1987, sect. 3, vol. IV, p. 297–339.
5. Gaston, B., J. M. Drazen, J. Loscalzo, and J. S. Stamler. The biology of nitrogen oxides in the airways. *Am. J. Respir. Crit. Med.* 149: 538–551, 1994.
6. George, S. C., J. E. Souders, A. L. Babb, and M. P. Hlastala. Modeling steady state inert gas exchange in the canine trachea. *J. Appl. Physiol.* 79: 929–940, 1995.
7. Guenard, H., N. Varene, and P. Vaida. Determination of lung capillary blood volume and membrane diffusing capacity in man by the measurement of NO and CO transfer. *Respir. Physiol.* 70: 113–120, 1987.
8. Gutierrez, H. H., B. R. Pitt, M. Schwarz, S. C. Watkins, C. Lowenstein, I. Caniggia, P. Chumley, and B. A. Freeman. Pulmonary alveolar epithelial inducible NO synthase gene expression: regulation by inflammatory mediators. *Am. J. Physiol.* 268 *(Lung Cell. Mol. Physiol.* 12): L501–L508, 1995.
9. Hildebrandt, J. Structural and mechanical aspects of respiration. In: *Textbook of Physiology*, edited by H. D. Patton, A. F.
Fuchs, B. Hille, A. M. Scher, and R. Steiner. Philadelphia, PA: Saunders, 1989, vol. 2, p. 991–1011.
10. Hogman, M., C. G. Frostell, H. Hedenstrom, and G. Hedenstierna. Inhalations of nitric oxide modulates adult human bronchial tone. *Am. Rev. Respir. Dis.* 148: 1474–1478, 1993.
11. Hyde, R. W., E. J. Geigel, A. J. Olszowka, J. A. Krasney, R. E. Forster, M. J. Utell, and M. W. Frampton. Determination of production of nitric oxide by lower airways—theory. *J. Appl. Physiol.* 82: 1290–1296, 1997.
12. Jia, L., C. Bonaventura, J. Bonaventura, and J. S. Stamler. *S*-nitrosohaemoglobin: a dynamic activity of blood involved in vascular control. *Nature* 380: 221–226, 1996.
13. Kharitonov, S. A., K. Alving, and P. J. Barnes. Exhaled and nasal nitric oxide measurements: recommendations. *Eur. Respir. J.* 10: 1683–1693, 1997.
14. Kharitonov, V. G., A. R. Sundquist, and V. S. Sharman. Kinetics of nitrosation of thiols by nitric oxide in the presence of oxygen. *J. Biol. Chem.* 270: 28158–28164, 1995.
15. Lancaster, J. R. Simulation of the diffusion and reaction of endogenously produced nitric oxide. *Proc. Natl. Acad. Sci. USA* 91: 8137–8141, 1994.
16. Malinski, T., Z. Taha, S. Grunfeld, S. Patton, M. Kapturczak, and P. Tombouliant. Diffusion of nitric oxide in the aorta wall monitored in situ by porphyrinic microsensors. *Biochem. Biophys. Res. Commun.* 193: 1076–1082, 1993.
17. Maroun, M. J., S. Mehta, R. Turcotte, M. G. Cosio, and S. N. A. Hussain. Effects of physical conditioning on endogenous nitric oxide output during exercise. *J. Appl. Physiol.* 79: 1219–1225, 1995.
18. Meyer, M., M. Mohr, H. Schulz, and J. Piiper. Sloping alveolar plateaus of CO_2, O_2, and intravenously infused C_2H_2 and $CHCIF_2$ in the dog. *Respir. Physiol.* 81: 137–152, 1990.
18a. National Research Council (U.S.). Solubilities of gases in water. In: *International Critical Tables of Numerical Data, Physics, Chemistry and Technology*, edited by E. Washburn, C. J. West, and N. E. Dorsey. New York: McGraw-Hill, 1928, p. 255–261.
19. Paiva, M., and L. A. Engel. The anatomical basis for the sloping N_2 plateau. *Respir. Physiol.* 44: 325–347, 1981.
20. Persson, M. G., N. P. Wiklund, and L. E. Gustafsson. Endogenous nitric oxide in single exhalations and the change during exercise. *Am. Rev. Respir. Dis.* 148: 1210–1214, 1993.
21. Phillips, C. R., G. D. Giraud, and W. E. Holden. Exhaled nitric oxide during exercise: site of release and modulation by ventilation and blood flow. *J. Appl. Physiol.* 80: 1865–1871, 1996.
22. Scherer, P. W., S. Gobran, S. J. Aukburg, J. E. Baumgardner, R. Bartkowski, and G. R. Neufeld. Numerical and experimental study of steady-state CO_2 and inert gas washout. *J. Appl. Physiol.* 64: 1022–1029, 1988.
23. Shaul, P. W., A. J. North, L. C. Wu, L. B. Wells, T. S. Brannon, K. S. Lau, T. Michel, L. R. Margraf, and R. A. Star. Endothelial nitric oxide synthase is expressed in cultured human bronchiolar epithelium. *J. Clin. Invest.* 94: 2231–2236, 1994.
24. Silkoff, P. E., P. A. McClean, A. S. Slutsky, H. G. Furlott, E. Hoffstein, S. Wakita, K. R. Chapman, J. P. Szalai, and N. Zamel. Marked flow dependence of exhaled nitric oxide using a new technique to exclude nasal nitric oxide. *Am. J. Respir. Crit. Med.* 155: 260–267, 1997.
25. Trolin, G., T. Anden, and G. Hedenstierna. Nitric oxide (NO) in expired air at rest and during exercise. *Acta Physiol. Scand.* 151: 159–163, 1994.
26. Tsoukias, N. M., Z. Tannus, A. F. Wilson, and S. C. George. Single-exhalation profiles of NO and CO_2 in humans: effect of dynamically changing flow rate. *J. Appl. Physiol.* 85: 642–652, 1998.
27. Weibel, E. *Morphometry of the Human Lung.* New York: Springer-Verlag, 1963.
28. Wood, J., and J. Garthwaite. Models of the diffusional spread of nitric oxide: implications for neural nitric oxide signalling and its pharmacological properties. *Neuropharmacology* 33: 1235–1244, 1994.